

# Theoretical results on the topological properties of the limited penetrable horizontal visibility graph family

Minggang Wang,<sup>1,2,3,\*</sup> André L.M.Vilela,<sup>3,4</sup> Ruijin Du,<sup>3,5</sup> Longfeng Zhao,<sup>3</sup> Gaogao Dong,<sup>3,5</sup> Lixin Tian,<sup>1,5,†</sup> and H. Eugene Stanley<sup>3</sup>

<sup>1</sup>*School of Mathematical Science, Nanjing Normal University, Nanjing 210042, Jiangsu, China*

<sup>2</sup>*Department of Mathematics, Nanjing Normal University Taizhou College, Taizhou 225300, Jiangsu, China*

<sup>3</sup>*Center for Polymer Studies and Department of Physics, Boston University, Boston, MA 02215, USA*

<sup>4</sup>*Universidade de Pernambuco, 50720-001, Recife-PE, Brazil*

<sup>5</sup>*Energy Development and Environmental Protection Strategy Research Center, Jiangsu University, Zhenjiang, 212013 Jiangsu, China*

The limited penetrable horizontal visibility graph algorithm was recently introduced to map time series in complex networks. We extend this visibility graph and create a directed limited penetrable horizontal visibility graph and an image limited penetrable horizontal visibility graph. We define the two algorithms and provide theoretical results on the topological properties of these graphs associated with different types of real-value series (or matrices). We perform several numerical simulations to further check the accuracy of our theoretical results. Finally we present an application of the directed limited penetrable horizontal visibility graph for measuring real-value time series irreversibility, and an application of the image limited penetrable horizontal visibility graph that discriminates noise from chaos. The empirical results show the effectiveness of our proposed algorithms.

PACS numbers: 05.45.Tp, 89.75.Hc, 05.45.-a

## I. INTRODUCTION

The complex network analysis of univariate (or multivariate) time series has recently attracted the attention of researchers working in a wide range of fields [1]. Over the past decade several methodologies have been proposed for mapping a univariate and multivariate time series in a complex network [2–9]. These include constructing a complex network from a pseudoperiodic time series [2], using a visibility graph (VG) algorithm [3], a recurrence network (RN) method [4], a stochastic processes method [5], a coarse geometry theory [6], a nonlinear mutual information method [7], event synchronization [8], and a phase-space coarse-graining method [9]. These methods have been widely used to solve problems in a variety of research fields [10–20].

Among all these time series complex network analysis algorithms, visibility algorithms [3, 21, 22] are the most efficient when constructing a complex network from a time series. Visibility algorithms are a family of rules for mapping a real-value time series on graphs that display several cases. In all cases each time series datum is assigned to a node, but the connection criterion differs. For example, in the natural visibility graph (NVG) two nodes  $i$  and  $j$  are connected if the geometrical criterion  $x(t_k) < x(t_i) + [x(t_j) - x(t_i)] \frac{t_k - t_i}{t_j - t_i}$ ,  $\forall t_k \in (t_i, t_j)$  is fulfilled within the time series [3]. In the parametric natural visibility graph

---

\*Electronic address: magic821204@sina.com, magic82@bu.edu

†Electronic address: tianlx@ujs.edu.cn

(PNVG) case there are three steps when using this algorithm to map a time series to a complex network, (i) build an NVG [3] as described above using common NVG criteria in the mapping, (ii) set the direction and angle,  $\alpha_{ij} = \arctan \frac{x(t_j) - x(t_i)}{t_j - t_i}$ ,  $i < j$  for every link of the NVG, and (iii) use the parameter view angle rule  $\alpha$ ,  $(i, j) \in PNVG(\alpha)$ ,  $\alpha_{ij} < \alpha$  to select links from the directed and weighted graph [21]. In the horizontal visibility graph (HVG) case, this algorithm is similar to the NVG algorithm but has a modified mapping criterion. Here two nodes  $i$  and  $j$  are connected if  $x(t_k) < \inf(x(t_i), x(t_j))$ ,  $\forall t_k \in (t_i, t_j)$  [22]. These visibility algorithms have been successfully implemented in a variety of fields [23–25].

Recently a limited penetrable visibility graph (LPVG) [26, 27] and a multiscale limited penetrable horizontal visibility graph (MLPHVG) [28] were developed from the visibility graph (VG) and the horizontal visibility graph (HVG) to analyze nonlinear time series. The LPVG and MLPHVG have been successfully used to analyze a variety of real signals across different fields, e.g., experimental flow signals [26-27], EEG signals [28, 29], and electromechanical signals [30]. Research has shown that the LPVG and MLPHVG inherit the merits of the VG, but also successfully screen out noise, which makes them particularly useful when analyzing signals polluted by unavoidable noise [26–30].

Abundant empirical results have already been obtained using the VG algorithm and its extensions, e.g., the PNVG [21], the HVG [22], the LPVG [26], and the MLPHVG [28]. Thus far there has been little research focusing on rigorous theoretical results. Recently Lacasa et al. presented topological properties of the horizontal visibility graph associated with random time series [22], periodic series [31], and other stochastic and chaotic processes [32]. They extended the family of visibility algorithms to map scalar fields of an arbitrary dimension onto graphs and provided analytical results on the topological properties of the graphs associated with different types of real-value matrices [33]. Wang et al. [34] focused on a class of general horizontal visibility algorithms, the limited penetrable horizontal visibility graph (LPHVG), and presented exact results on the topological properties of the limited penetrable horizontal visibility graph associated with a random series. Here we use the previous works [22, 31–34], focus our attention on the limited penetrable horizontal visibility graph, and present some analytical properties.

This paper is organized as follows. In Section II of this paper we introduce the limited penetrable horizontal visibility graph family. In Section III we derive the analytical properties of the different versions of associated limited penetrable horizontal visibility graphs of a generic random time series (or a random matrix) and present several numerical simulations to check their accuracy. In Section IV we show some applications of the directed limited penetrable horizontal visibility graph and the image limited penetrable horizontal visibility graph. In Section V we present our conclusions.

## II. LIMITED PENETRABLE HORIZONTAL VISIBILITY GRAPH FAMILY

The LPHVG algorithm [28, 34] and its extensions are called the LPHVG family. We here present three versions of the LPHVG algorithm, the limited penetrable horizontal visibility graph, LPHVG( $\rho$ ), the directed limited penetrable horizontal visibility graph, DLPHVG( $\rho$ ), and the image limited penetrable horizontal visibility graph of order  $n$ , ILPHVG $_n$ ( $\rho$ ).

### A. Limited Penetrable Horizontal Visibility Graph [LPHVG( $\rho$ )]

The limited penetrable horizontal visibility graph [LPHVG( $\rho$ )] [34] is a geometrically simpler and analytically solvable version of VG [3], LPVG [30], and MLPHVG [28]. To define it we let  $\{x_i\}_{i=1,2,\dots,N}$  be a time series of  $N$  real numbers. We set the limited penetrable distance to  $\rho$ , and LPHVG( $\rho$ ) maps the time series on a graph with  $N$  nodes and an adjacency matrix **A**. Nodes  $x_i$  and  $x_j$  are connected through an undirected edge ( $A_{ij} = A_{ji} = 1$ ) if  $x_i$  and  $x_j$  have a limited penetrable horizontal

visibility (see Fig. 1), i.e., if  $\rho \geq 0$  intermediate data  $x_q$  follows

$$x_q \geq \inf\{x_i, x_j\}, \forall q \in (i, j), \aleph(q) \leq \rho, \quad (1)$$

where  $\aleph(q)$  is the number of  $q$ . The graph spanned by this mapping is the limited penetrable horizontal visibility graph [LPHVG( $\rho$ )]. When we set the limited penetrable distance  $\rho$  to 0, then LPHVG(0) degenerates into an HVG [22], i.e., LPHVG(0) = HVG. When  $\rho \neq 0$  there are more connections between any two LPHVG( $\rho$ ) nodes than in HVG. Fig. 1(b) shows the new established connections (red lines) when we infer the LPHVG(1) using HVG. Note that the LPHVG( $\rho$ ) of a time series has all the properties of its corresponding HVG, e.g., it is connected and invariant under affine transformations of series data [22].

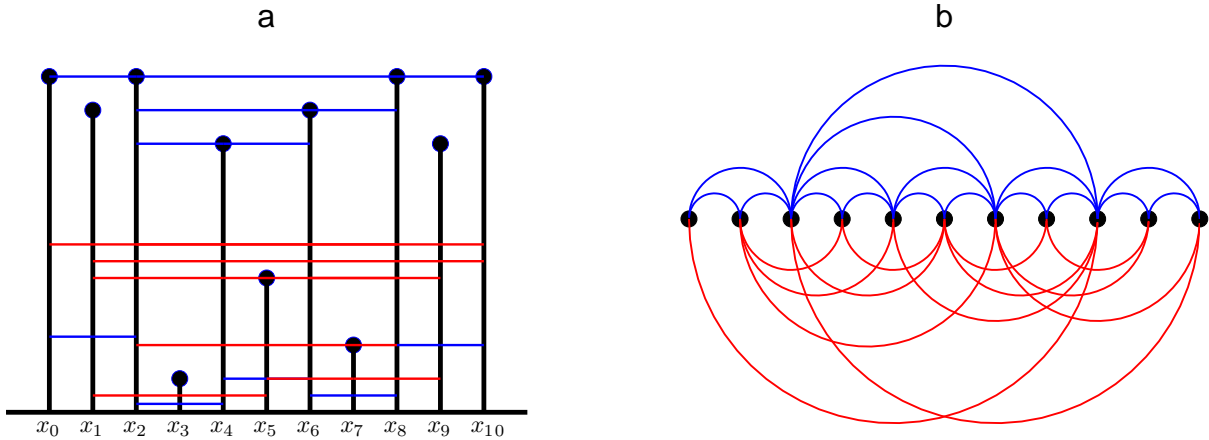


FIG. 1: Example of (a) a time series (11 data values) and (b) its corresponding LPHVG(1), where every node corresponds to time series data in the same order. The horizontal penetrable visibility lines between data points define the links connecting nodes in the graph.

### B. Directed limited penetrable horizontal visibility graph [DLPHVG( $\rho$ )]

The limited penetrable horizontal visibility graph [LPHVG( $\rho$ )] is undirected, because penetrable visibility does not have a predefined temporal arrow. Directionality can be added by using directed networks. Here we address the directed version and define a directed limited penetrable horizontal visibility graph [DLPHVG( $\rho$ )], where the degree  $k(x_t)$  of the node  $x_t$  is split between an ingoing degree  $k_{\text{in}}(x_t)$  and an outgoing degree  $k_{\text{out}}(x_t)$  such that  $k(x_t) = k_{\text{in}}(x_t) + k_{\text{out}}(x_t)$ . We define the ingoing degree  $k_{\text{in}}(x_t)$  to be the number of links of node  $x_t$  with past nodes associated with data in the series, i.e., nodes with  $t' < t$ . Conversely, we define the outgoing degree  $k_{\text{out}}(x_t)$  to be the number of links with future nodes, i.e., nodes with  $t'' > t$ . Thus DLPHVG( $\rho$ ) maps the time series into a graph with  $N$  nodes and an adjacency matrix  $\mathbf{A} = \mathbf{A}_{\text{in}} + \mathbf{A}_{\text{out}}$ , where  $\mathbf{A}_{\text{in}}$  is a lower triangular matrix and  $\mathbf{A}_{\text{out}}$  is an upper triangular matrix. Nodes  $x_{t'}$  and  $x_t$ ,  $t' < t$  (or  $x_t$  and  $x_{t''}$ ,  $t < t''$ ) are connected through a directed edge  $x_{t'} \rightarrow x_t$ , i.e.,  $A_{t't} = 1$  (or  $x_t \rightarrow x_{t''}$ , i.e.  $A_{tt''} = 1$ ) if it satisfies Eq. (1).

Fig. 2 shows a graphical representation of the definition. As in the degree distribution  $P(k)$ , we use the ingoing and outgoing degree distributions of a DLPHVG( $\rho$ ) to define the probability distributions of  $k_{\text{out}}$  and  $k_{\text{in}}$  on the graph, which are  $P_{\text{out}}(k) \equiv$

$P(k_{\text{out}} = k)$  and  $P_{\text{in}}(k) \equiv P(k_{\text{in}} = k)$ , respectively. We see the asymmetry of the resulting graph in a first approximation when we use the invariance of the outgoing (or ingoing) degree series under a time reversal.

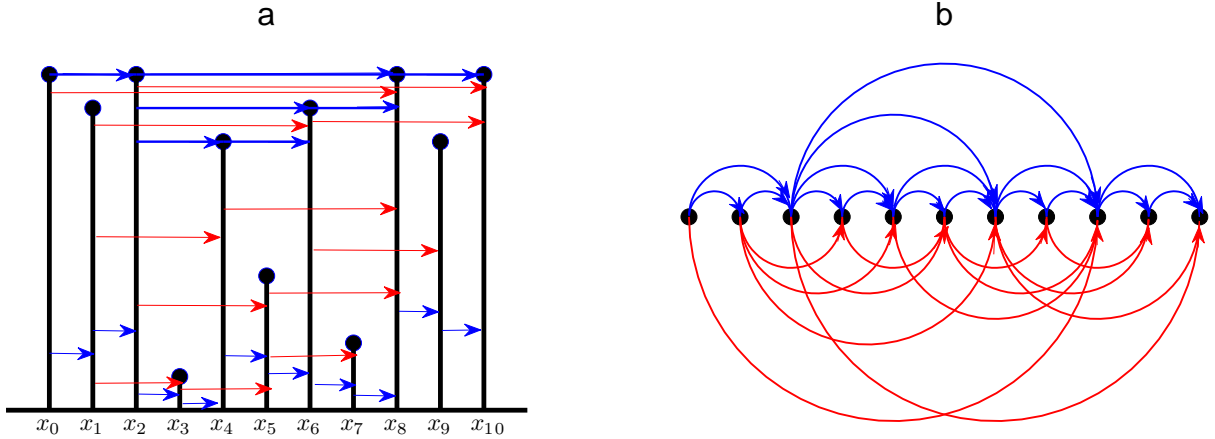


FIG. 2: Graphical illustration of DLPHVG(1). (a) Plot of a sample time series  $\{x_t\}, t = 0, 1, 2, \dots, 10$ . Each datum in the series is mapped to a node in the graph. Arrows, describing allowed directed penetrable visibility, link nodes. (b) Plot of the associated DLPHVG(1). In this graph, each node has an ingoing degree  $k_{\text{in}}$ , which accounts for the number of links with past nodes, and an outgoing degree  $k_{\text{out}}$ , which in turn accounts for the number of links with future nodes.

### C. Image limited penetrable horizontal visibility graph of order $n$ [ILPHVG $_n(\rho)$ ]

One-dimensional versions of the limited penetrable horizontal visibility graph [LPHVG( $\rho$ )] and directed limited penetrable horizontal visibility graph [DLPHVG( $\rho$ )] are used to map landscapes (time series) on complex networks. As in the definition of  $\text{IVG}_n$  [33], the definition of LPHVG( $\rho$ ) can also be extended and applied to two-dimensional manifolds by extending the LPHVG( $\rho$ ) criteria of Eq. (1) along one-dimensional sections of the manifold. To define the image limited penetrable horizontal visibility graph of order  $n$  [ILPHVG $_n(\rho)$ ] we let  $\mathbf{X}$  be a  $N \times N$  matrix for an arbitrary entry  $(i, j)$  and partition the plane into  $n$  directions such that direction  $p$  is at an angle with the row axis of  $2\pi(p-1)/n$ , where  $p = 1, 2, \dots, n$ . The image limited penetrable visibility graph of order  $n$ , ILPHVG $_n(\rho)$ , has  $N^2$  nodes, each of which is labeled using a duple  $(i, j)$  associated with the entry indices  $x_{ij}$ , such that two nodes,  $x_{ij}$  and  $x_{i'j'}$ , are linked when (i)  $x_{i'j'}$  belongs to one of the  $n$  angular partition lines, and (ii)  $x_{ij}$  and  $x_{i'j'}$  are linked in the LPHVG( $\rho$ ) defined over the ordered sequence that includes  $(i, j)$  and  $(i', j')$ . For example, in ILPHVG $_4(1)$  the penetrable visibility between two points  $x_{ij}$  and  $x_{i'j'}$  is

$$i = i', x_{iq} \geq \text{inf}\{x_{ij}, x_{i'j'}\}, \forall q \in (j, j'), \aleph(q) \leq \rho, \quad (2)$$

or

$$j = j', x_{qj} \geq \text{inf}\{x_{ij}, x_{i'j'}\}, \forall q \in (i, i'), \aleph(q) \leq \rho. \quad (3)$$

Fig. 3(a) shows a sample matrix in which  $x_0$  is the central entry, which shows the ILPHVG $_4(1)$  algorithm evaluated along the vertical and horizontal directions. Fig. 3(b) shows the connectivity pattern associated to the entry  $x_0$  of the ILPHVG $_4(1)$

algorithm. Fig. 3(c) shows the  $\text{ILPHVG}_8(1)$  algorithm evaluated along the vertical, horizontal, and diagonal directions. Fig. 3(d) shows the connectivity pattern associated to the entry  $x_0$  of the  $\text{ILPHVG}_8(1)$  algorithm.

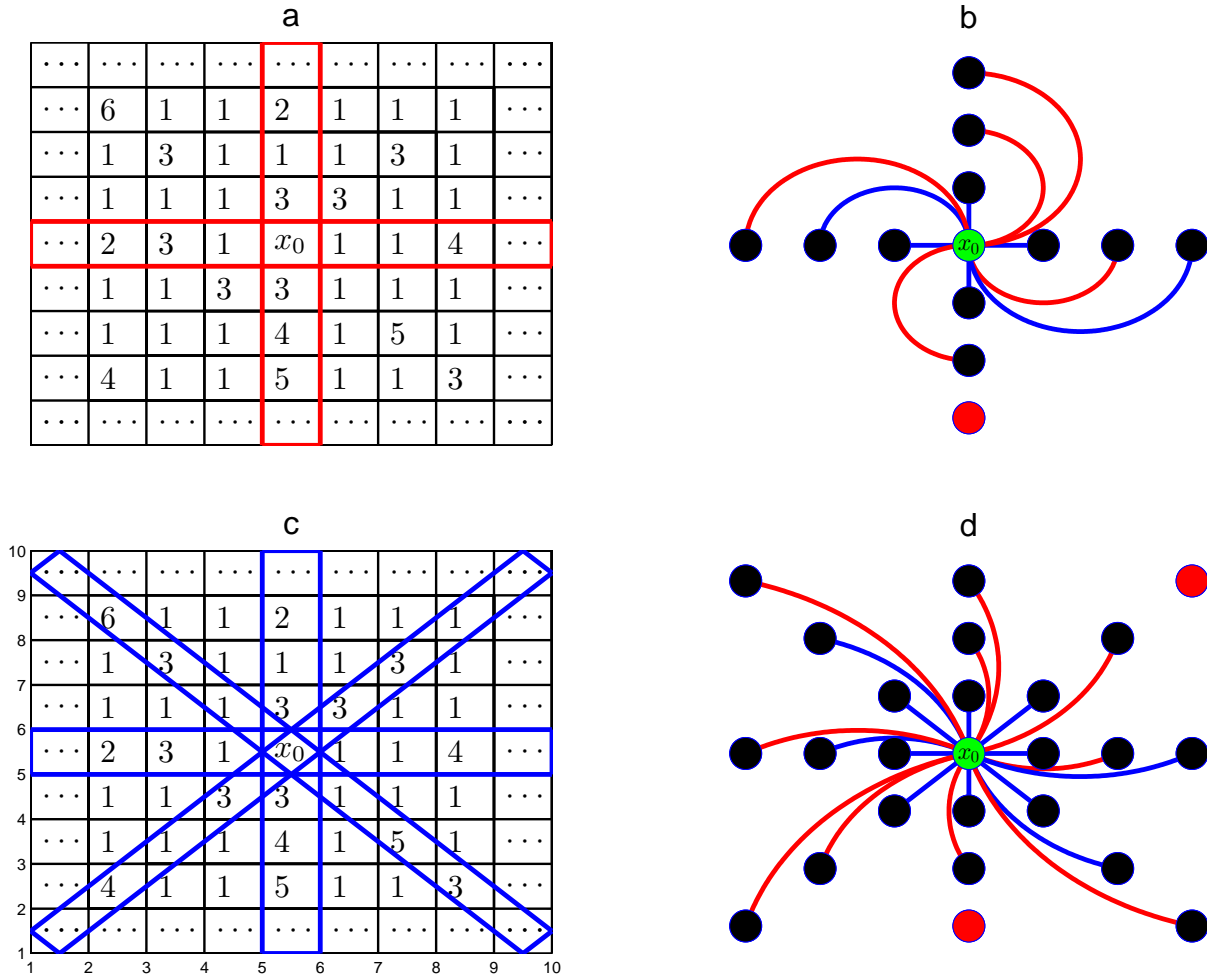


FIG. 3: Graphical illustration of  $\text{ILPHVG}_n(\rho)$ . In Fig. 3(a) we depict a sample matrix where  $x_0 = 2$  is the central entry, which shows the  $\text{ILPHVG}_4(1)$  algorithm is evaluated along the vertical and horizontal directions, and in Fig. 3(b) of the same figure we describe the connectivity pattern associated to this entry  $x_0$  in the case of  $\text{ILPHVG}_4(1)$ . Fig. 3(c) shows the  $\text{ILPHVG}_8(1)$  algorithm is evaluated both along the vertical and horizontal directions and along the diagonals directions, and in Fig. 3(d) of the same figure we describe the connectivity pattern associated to this entry  $x_0$ .

### III. THEORETICAL RESULTS ON THE TOPOLOGICAL PROPERTIES

**Theorem 1. [34]** If we let  $X(t)$  be a bi-infinite sequence of *i.i.d.*, a random variable  $X$  with probability density  $f(x)$ , then the degree distribution of its associated LPHVG( $\rho$ ) is

$$P(k) = \begin{cases} \frac{1}{2\rho+3} \left(\frac{2\rho+2}{2\rho+3}\right)^{k-2(\rho+1)}, & k \geq 2\rho + 2. \\ 0, & \text{otherwise.} \end{cases}$$

The mean degree  $\langle k \rangle$  is

$$\langle k \rangle = 4(\rho + 1).$$

Reference [34] [Wang et al., 2017] provides a lengthy proof of this theorem. We here propose an alternative shorter proof.

**Proof.** We let  $x$  be an arbitrary datum of the *i.i.d.* random time series. The probability that its limited penetrable horizontal visibility is interrupted by two bounding data, one datum  $x_{bl}$  on its left and one  $x_{br}$  on its right. There are  $2\rho$  penetrable data that are larger than  $x$  between the two bounding data,  $\rho$  penetrable data  $x_{pl}^1, x_{pl}^2, \dots, x_{pl}^\rho$  on the left and  $\rho$  data  $x_{pr}^1, x_{pr}^2, \dots, x_{pr}^\rho$  on the right of  $x$ . These  $2\rho + 2$  data are independent of  $f(x)$ , then

$$\begin{aligned} \Phi_{2\rho+2} = & \int_{-\infty}^{\infty} \int_x^{\infty} \int_x^{\infty} \int_x^{\infty} \dots \int_x^{\infty} \int_x^{\infty} \dots \int_x^{\infty} f(x)f(x_{bl})f(x_{br})f(x_{pl}^1)\dots f(x_{pl}^\rho)f(x_{pr}^1)\dots f(x_{pr}^\rho)dx_{pr}^\rho \dots \\ & \dots dx_{pr}^1 dx_{pl}^\rho \dots dx_{pl}^1 dx_{br} dx_{bl} dx. \end{aligned} \quad (4)$$

We define the cumulative probability distribution function  $F(x)$  of any probability distribution  $f(x)$  to be

$$F(x) = \int_{-\infty}^x f(t)dt. \quad (5)$$

Then we rewrite Eq. (4) to be

$$\Phi_{2\rho+2} = \int_{-\infty}^{\infty} f(x)[1 - F(x)]^{2\rho+2} dx = \frac{1}{2\rho+3}. \quad (6)$$

The probability  $P(k)$  that the datum penetrates no more than  $\rho$  time seeing  $k$  data is

$$P(k) = \Phi(k)\Phi_{2\rho+2} = \frac{1}{2\rho+3}\Phi(k), \quad (7)$$

where  $\Phi(k)$  is the probability that datum  $x$  penetrates no more than  $\rho$  time seeing at least  $k$  data. We can recurrently calculate  $\Phi(k)$  to be

$$\Phi(k) = \Phi(k-1)(1 - \Phi_{2\rho+2}) = \frac{2\rho+2}{2\rho+3}\Phi(k-1), \quad \Phi(2\rho+2) = 1, \quad (8)$$

from which we deduce

$$\Phi(k) = \left(\frac{2\rho+2}{2\rho+3}\right)^{k-2(\rho+1)}\Phi(2\rho+2) = \left(\frac{2\rho+2}{2\rho+3}\right)^{k-2(\rho+1)}. \quad (9)$$

Thus we finally obtain

$$P(k) = \begin{cases} \Phi(k)\Phi_{2\rho+2} = \frac{1}{2\rho+3} \left(\frac{2\rho+2}{2\rho+3}\right)^{k-2(\rho+1)}, & k \geq 2\rho + 2, \\ 0, & \text{otherwise,} \end{cases} \quad \rho = 0, 1, 2, \dots \quad (10)$$

Then the mean degree  $\langle k \rangle$  of the limited penetrable horizontal visibility graph associated to an uncorrelated random process is

$$\langle k \rangle = \sum_{k=2\rho+2}^{\infty} kP(k) = \sum_{k=2\rho+2}^{\infty} \frac{k}{2\rho+3} \left(\frac{2\rho+2}{2\rho+3}\right)^{k-2(\rho+1)} = 4(\rho+1). \quad (11)$$

Theorem 1 shows the exact degree distribution for LPHVG( $\rho$ ), which indicates that the degree distribution  $P(k)$  of LPHVG( $\rho$ ) associated to *i.i.d.* random time series has a unified exponential form, independent of the probability distribution from which the series was generated.

**Theorem 2.** We let  $X(t)$  be a bi-infinite sequence of *i.i.d.*, a random variable  $X$  with probability density  $f(x)$ , and consider a limited penetrable horizontal visibility graph associated with  $X(t)$ . We let  $\langle K(x) \rangle$  be a mean degree of the node associated with a datum of height  $x$  and define it

$$\langle K(x) \rangle = 2(\rho+1) - 2(\rho+1)\ln(1-F(x)), F(x) = \int_{-\infty}^x f(t)dt.$$

**Proof.** We define  $P(k|x)$  to be the conditional probability that a given node has degree  $k$  when its height is  $x$ . Using the constructive proof process of  $P(k)$  in Ref. [34] [Wang et al., 2017], we calculate  $P(k|x)$  to be

$$\begin{aligned} P(k|x) &= \sum_{h=0}^{k-2(\rho+1)} (2\rho+1)^h \frac{(-1)^{k-2(\rho+1)}}{h! [k-2(\rho+1)-h]!} [1-F(x)]^{2(\rho+1)} [\ln(1-F(x))]^{k-2(\rho+1)} \\ &= [1-F(x)]^{2(\rho+1)} [2(\rho+1)\ln(1-F(x))]^{k-2(\rho+1)} \frac{(-1)^{k-2(\rho+1)}}{[k-2(\rho+1)]!}. \end{aligned} \quad (12)$$

Then  $\langle K(x) \rangle$  is

$$\langle K(x) \rangle = \sum_{k=2(\rho+1)}^{\infty} kP(k|x). \quad (13)$$

We let  $k-2(\rho+1) = \alpha$ ,  $2(\rho+1)\ln[1-F(x)] = A$  and deduce

$$\begin{aligned} \langle K(x) \rangle &= 2(\rho+1)[1-F(x)]^{2(\rho+1)} \sum_{\alpha=0}^{\infty} \frac{(-1)^\alpha A^\alpha}{\alpha!} + [1-F(x)]^{2(\rho+1)} \sum_{\alpha=1}^{\infty} \frac{(-1)^\alpha A^\alpha}{(\alpha-1)!} \\ &= 2(\rho+1) - A = 2(\rho+1) - 2(\rho+1)\ln[1-F(x)]. \end{aligned} \quad (14)$$

Theorem 2 shows the relation between data height  $x$  and the mean degree of the nodes associated with the data of height  $x$ . The result indicates that the  $\langle K(x) \rangle$  is a monotonically increasing function of  $x$ . Thus we conclude that the hubs of LPHVG( $\rho$ ) are the data with largest values. We check the accuracy of the result within finite series. Fig. 4(a) shows a plot of the numerical values of  $\langle K(x) \rangle$  of LPHVG( $\rho$ ),  $\rho = 0, 2, 4, 6, 8, 10$  associated with the random series of 1000 data extracted from a uniform distribution when  $F(x) = x$ . The theoretical results (red lines) show a perfect agreement [Eq. (14)]. To check the finite size effect, Fig. 4(b) shows a plot of the numerical values of  $\langle K(x) \rangle$  of LPHVG(2) associated with random series of 500, 1000, 1500, 2000 data. We use root mean square error (RMSE) to measure the agreement between the numerical and theoretical results. We find that when the size  $N$  of the time series increases, the RMSE between the numerical and theoretical results decreases, indicating an increase in agreement.

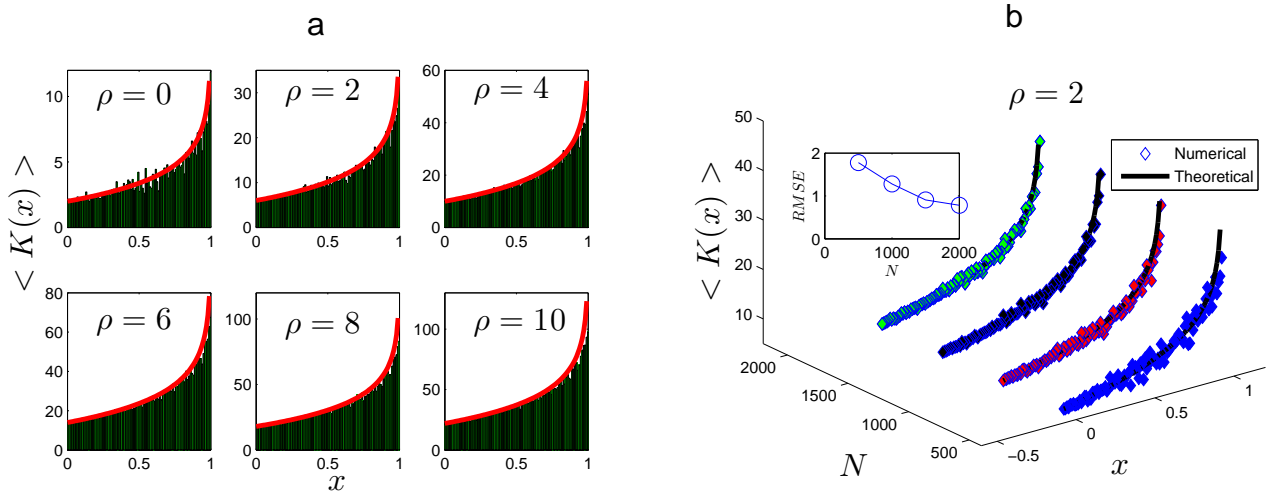


FIG. 4: (a) The relation between data height  $x$  and the node degree  $\langle K(x) \rangle$  under different penetrable distance  $\rho$ . (b) the relation between data height  $x$  and the node degree  $\langle K(x) \rangle$  under different time series size  $N$ .

**Theorem 3.** We let  $X_t$  be an infinite periodic series of period  $T$  with no repeated values within a period. The normalized mean distance  $\langle d \rangle$  of LPHVG( $\rho$ ) associated with  $X_t$  is

$$\langle d \rangle \sim [4(\rho + 1) - \langle k(T) \rangle],$$

where

$$\langle k(T) \rangle = 4(\rho + 1) \left(1 - \frac{2\rho + 1}{2T}\right), \rho \ll T.$$

**Proof.** To calculate  $\langle k(T) \rangle$  we consider an infinite periodic series of period  $T$  with no repeated values in a period and denote it  $X_t = \{\dots, x_0, x_1, x_2, \dots, x_T, x_1, x_2, \dots\}$ ,  $x_0 = x_T$ . We let  $\rho \ll T$  for the subseries  $\tilde{X}_t = \{x_0, x_1, x_2, \dots, x_T\}$  and without losing generality assume that  $x_0 = x_T$  corresponds to the largest value of the subseries,  $x_1, \dots, x_\rho, x_{T-\rho}, \dots, x_{T-1}$ , and corresponds to the 2nd to  $(2\rho + 1)$ nd largest value of the subseries. Thus we construct the LPHVG( $\rho$ ) associated with subseries  $\tilde{X}_t$ . We assume that LPHVG( $\rho$ ) has  $E$  links and let  $x_i$  be the smallest datum of the subseries  $\tilde{X}_t$ . Because no data repetitions are allowed in  $\tilde{X}_t$ , the degree of  $x_i$  is  $2(\rho + 1)$  when constructed from LPHVG( $\rho$ ). We now remove node  $x_i$  and its  $2(\rho + 1)$  links from LPHVG( $\rho$ ). The resulting graph now has  $E - 2(\rho + 1)$  links and  $T$  nodes. We iterate this operation  $T - (2\rho + 1)$  times. The resulting graph has  $2(\rho + 1)$  nodes, i.e.,  $x_0, x_1, \dots, x_\rho, x_{T-\rho}, \dots, x_{T-1}, x_T$ . When these  $2(\rho + 1)$  nodes are connected by  $E_r = \binom{2\rho+2}{2}$  links, the total number of deleted links are  $E_d = 2(\rho + 1)[T - (2\rho + 1)]$ . Thus the mean degree of a limited penetrable horizontal visibility graph associated with  $X_t$  is

$$\langle k(T) \rangle = 2 \frac{E_d + E_r}{T} = \frac{2[(2(\rho + 1))(T - (2\rho + 1)) + (\rho + 1)(2\rho + 1)]}{T} = 4(\rho + 1) \left(1 - \frac{2\rho + 1}{2T}\right), \rho \ll T. \quad (15)$$

We let  $\langle d \rangle$  be the mean distance of LPHVG( $\rho$ ),  $N$  be the number of nodes, and the normalized mean distance  $\langle d \rangle$  be  $\langle d \rangle = \frac{\langle d \rangle}{N}$ . Note that  $\langle d \rangle$  depends on  $T$  for HVG associated with periodic orbits  $\langle d \rangle \sim T^{-1}$  for  $N \rightarrow \infty$  [31]. Thus we deduce that  $\langle d \rangle \sim T^{-1}$  for LPHVG( $\rho$ ). Using Eq. (15) we obtain  $T^{-1} \sim [4(\rho + 1) - \langle k(T) \rangle]$ , and finally obtain

$$\langle d \rangle \sim [4(\rho + 1) - \langle k(T) \rangle]. \quad (16)$$



This result holds for every periodic or aperiodic series ( $T \rightarrow \infty$ ), independent of the deterministic process that generates them, because the only constraint in its derivation is that data within a period not be repeated. Note that one consequence of Eq. (15) is that each time series has an associated LPHVG( $\rho$ ) with a maximum mean degree (for a aperiodic series) of  $\langle k(\infty) \rangle = 4(\rho + 1)$ , which agrees with the previous result in Eq. (11). In Eq. (16) the limiting solution  $\langle k(T) \rangle \rightarrow 4(\rho + 1)$ ,  $\langle d \rangle \rightarrow 0$  holds for all aperiodic, chaotic, and random series. To check the accuracy of the analytical result, we generate four periodic time series ( $T = 50, 100, 200$ , and  $250$ ) with 2000 data points. The data in each period is from the logistic map in which  $\mu = 4$ . We construct the limited penetrable horizontal visibility graphs with penetrable distance  $\rho = 0, 1, 2, \dots, 10$  associated with this periodic time series. Fig. 5(a) shows a plot of the mean degree of the resulting LPHVG( $\rho$ ) values with different  $\rho$  values that indicate a good agreement with the theoretical results in Eq. (15). Fig. 5(b) shows a calculation of the normalized mean distance  $\langle d \rangle$  of LPHVG( $\rho$ ) values with  $\rho = 0, 1$ , and  $2$  associated with the period time series of  $T = 100, 200, \dots, 1000$ . Numerical values of the mean normalized distance  $\langle d \rangle$  as a function of mean degree  $\langle k(T) \rangle$  agrees with the theoretical linear relation of Eq. (16).

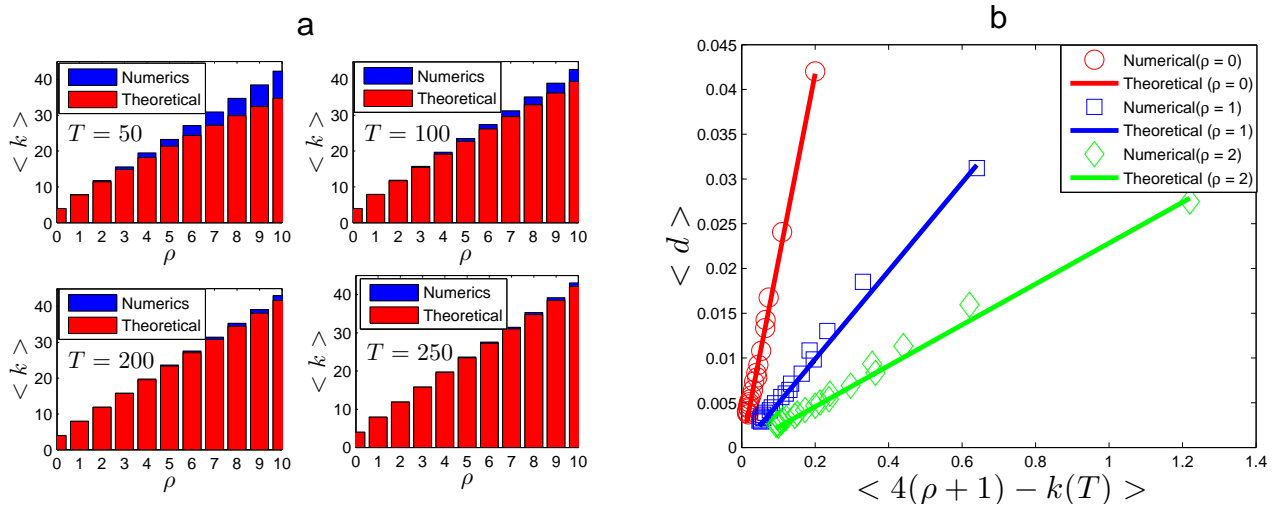


FIG. 5: ( a ) Numerical result of Eq. (15), we simulated the period time series ( $T = 50, 100, 200, 250$  respectively ) with 2000 data points are generated ( the data in each period from the Logistic map with  $\mu = 4$  ), ( b ) Numerical result of Eq. (16), we simulated the period time series with  $T = 100, 200, \dots, 1000$ .

**Theorem 4.** [34] We let  $X(t)$  be a real value bi-infinite time series of *i.i.d.* random variables  $X$  with probability distribution  $f(x)$  and examine its associated LPHVG( $\rho$ ). The local clustering coefficient distribution is then

$$P(C_{\min}) = \frac{1}{2\rho+3} \exp\left\{\left[\frac{\varphi + \sqrt{\varphi^2 - 8C_{\min}(2\rho+1)}}{2C_{\min}} - 2(\rho+1)\right] \ln\left(\frac{2\rho+2}{2\rho+3}\right)\right\}$$

and

$$P(C_{\max}) = \frac{1}{2\rho+3} \exp\left\{\left[\frac{\phi + \sqrt{\phi^2 - 8C_{\max}(6\rho+1)}}{2C_{\max}} - 2(\rho+1)\right] \ln\left(\frac{2\rho+2}{2\rho+3}\right)\right\}.$$

**Theorem 5.** [34] We let  $\{x_t\}_{t=0,1,\dots,N}$  be a bi-finite sequence of *i.i.d.* random variables extracted from a continuous probability density  $f(x)$ . Then the probability  $P_\rho(n)$  that two data separated by  $n$  intermediate data are two connected nodes in the

LPHVG( $\rho$ ) is

$$P_\rho(n) = \frac{2\rho(\rho+1)+2}{n(n+1)}, \rho = 0, 1, 2, \dots$$

Theorem 4 shows the distribution characteristics of the minimum clustering coefficient and the maximum clustering coefficient of the nodes in LPHVG( $\rho$ ). Theorem 5 indicates that the limited penetrable visibility probability  $P_\rho(n) = \frac{2\rho(\rho+1)+2}{n(n+1)}$  introduces shortcuts in the LPHVG( $\rho$ ). With these shortcuts the limited penetrable horizontal visibility graph reveals the presence of small-world phenomena [34].

**Theorem 6.** We let  $X(t)$  be a bi-infinite sequence of *i.i.d.* of random variable  $X$  with a probability density  $f(x)$ . Then both the in and out degree distribution of its associated DLPHVG( $\rho$ ) is

$$P_{\text{in}}(k) = P_{\text{out}}(k) = \begin{cases} \frac{1}{\rho+2} \left(\frac{\rho+1}{\rho+2}\right)^{k-(\rho+1)}, & k \geq \rho + 1. \\ 0, & \text{otherwise.} \end{cases}$$

**Proof.** Examining the out-distribution  $P_{\text{out}}(k)$  we let  $x$  be an arbitrary datum of the *i.i.d.* random time series, and  $x_{br} \geq x$  the probability that its limited penetrable horizontal visibility is interrupted by one bounding datum on its right. There are  $\rho$  penetrable data  $x_{p1}, x_{p2}, \dots, x_{p\rho} \geq x$  between  $x$  and the bounding data  $x_{br}$ . These  $\rho + 1$  data are independent of  $f(x)$ . Then

$$\begin{aligned} D\Phi_{\text{out}}^{\rho+1} &= \int_{-\infty}^{\infty} \int_x^{\infty} \dots \int_x^{\infty} \int_x^{\infty} f(x)f(x_{p1})\dots f(x_{p\rho})f(x_{br})dx_{br}dx_{p\rho}\dots dx_{p1}dx \\ &= \int_{-\infty}^{\infty} f(x)[1 - F(x)]^{\rho+1}dx = \frac{1}{\rho+2}. \end{aligned} \quad (17)$$

The probability  $P_{\text{out}}(k)$  that datum  $x$  penetrates no more than  $\rho$  time seeing  $k$  data is

$$P_{\text{out}}(k) = D\Phi_{\text{out}}(k)D\Phi_{\text{out}}^{\rho+1} = \frac{1}{\rho+2}D\Phi_{\text{out}}(k), \quad (18)$$

where  $D\Phi(k)$  is the probability that  $x$  penetrates no more than  $\rho$  time to the right seeing at least  $k$  data. Then  $D\Phi(k)$  can be recurrently calculated

$$D\Phi(k) = D\Phi(k-1)(1 - D\Phi_{\text{out}}^{\rho+1}) = \frac{\rho+1}{\rho+2}D\Phi(k-1) = \left(\frac{\rho+1}{\rho+2}\right)^{k-(\rho+1)}D\Phi(\rho+1), \quad (19)$$

from which, with  $D\Phi(\rho+1) = 1$ , we deduce

$$D\Phi(k) = \left(\frac{\rho+1}{\rho+2}\right)^{k-(\rho+1)}. \quad (20)$$

Thus we finally obtain

$$P_{\text{out}}(k) = D\Phi_{\text{out}}(k)D\Phi_{\text{out}}^{\rho+1} = \begin{cases} \frac{1}{\rho+2} \left(\frac{\rho+1}{\rho+2}\right)^{k-(\rho+1)}. \\ 0, & \text{otherwise.} \end{cases} \quad (21)$$

To further check the accuracy of Eq. (21), we perform several numerical simulations. We generate random series of 3000 data from uniform, gaussian, and power law distributions and their associated DLPHVG( $\rho$ ). Fig. 6 show plots of the degree distributions with penetrable distances  $\rho = 0, 1, \text{ and } 2$ . Circles indicate  $P_{\text{in}}(k)$ , diamonds  $P_{\text{out}}(k)$ , and the solid line the theoretical results of Eq. (21). We find that the theoretical results agree with the numerics, placing aside finite size effects. As in the degree distribution of LPHVG( $\rho$ ) [34], the deviations between the tails of the in and out degree distributions of DLPHVG( $\rho$ ) associated with *i.i.d.* random series are caused solely by finite size effects.

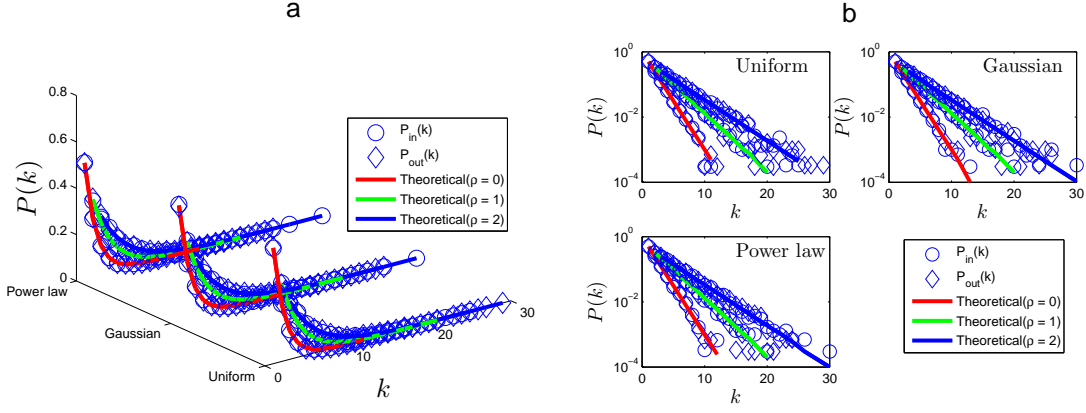


FIG. 6: (a) Plot of the in and out degree distribution of the resulting graphs, (b) semi-log plot of the in and out degree distribution of the resulting graphs.

**Theorem 7.** We let  $\mathbf{X}_{N \times N}$  be a matrix with entries  $x_{ij} = \xi$ , where  $\xi$  is a random variable sampled from a distribution  $f(x)$ . Then when  $n > 0$  and in the limited  $N \rightarrow \infty$ , the degree distribution of the associated ILPHVG $_n(\rho)$  converges to

$$P(k) = \begin{cases} \frac{1}{[n(\rho+1)+1]} \left[ \frac{n(\rho+1)}{n(\rho+1)+1} \right]^{k-n(\rho+1)}, & k \geq n(\rho+1). \\ 0, & \text{otherwise.} \end{cases}$$

**Proof.** To derive general results, we consider the two special cases  $n = 4$  and  $n = 8$ .

In the case  $n = 4$ , we let  $x$  be an arbitrary datum in  $\mathbf{R}_{N \times N}$  where the probability of its image limited penetrable horizontal visibility is interrupted by four bounding datum, i.e.,  $x_{br}$  on its right,  $x_{bu}$  above it,  $x_{bl}$  on its left, and  $x_{bb}$  below it. There are  $4\rho$  penetrable data  $x_{pr1}, \dots, x_{pr\rho}, x_{pu1}, \dots, x_{pu\rho}, x_{pl1}, \dots, x_{pl\rho}, x_{pb1}, \dots, x_{pb\rho}$  between  $x$  and the four bounding data. These  $4\rho + 4$  data are independent of  $f(x)$ . Then

$$\begin{aligned} I\Phi[4(\rho+1)] &= \int_{-\infty}^{\infty} \int_x^{\infty} \dots \int_x^{\infty} \int_x^{\infty} \dots \int_x^{\infty} \int_x^{\infty} \dots \int_x^{\infty} \int_x^{\infty} \dots \int_x^{\infty} \int_x^{\infty} \int_x^{\infty} \int_x^{\infty} f(x) f(x_{pr1}) \dots f(x_{pr\rho}) f(x_{pu1}) \dots \\ &\dots f(x_{pu\rho}) f(x_{pl1}) \dots f(x_{pl\rho}) f(x_{pb1}) \dots f(x_{pb\rho}) f(x_{br}) f(x_{bu}) f(x_{bl}) f(x_{bb}) dx_{bb} dx_{bl} dx_{bu} dx_{br} dx_{pb\rho} \dots \\ &\dots dx_{pb1} dx_{pl\rho} \dots dx_{pl1} dx_{pu\rho} \dots dx_{pu1} dx_{pr\rho} \dots dx_{pr1} dx \\ &= \int_{-\infty}^{\infty} f(x) [1 - F(x)]^{4\rho+4} dx = \frac{1}{4\rho+5}. \end{aligned} \quad (22)$$

The probability that the node  $x$  has a penetrable visibility of exactly  $k$  nodes is

$$P(k) = \{1 - I\Phi[4(\rho+1)]\}^{k-4(\rho+1)} I\Phi[4(\rho+1)] = \frac{1}{4\rho+5} \left( \frac{4\rho+4}{4\rho+5} \right)^{k-4(\rho+1)}, \quad k \geq 4(\rho+1). \quad (23)$$

Similarly, when  $n = 8$  from Eq. (22), then

$$I\Phi[8(\rho+1)] = \int_{-\infty}^{\infty} f(x) [1 - F(x)]^{8\rho+8} dx = \frac{1}{8\rho+9}. \quad (24)$$

Here the probability that node  $x$  has a penetrable visibility of exactly  $k$  nodes is

$$P(k) = \{1 - I\Phi[8(\rho+1)]\}^{k-8(\rho+1)} I\Phi[8(\rho+1)] = \frac{1}{8\rho+9} \left( \frac{8\rho+8}{8\rho+9} \right)^{k-8(\rho+1)}, \quad k \geq 8(\rho+1). \quad (25)$$

From Eqs. (23) and (25) we deduce a generic  $n$  that yields

$$P(k) = \{1 - I\Phi[n(\rho + 1)]\}^{k-n(\rho+1)} I\Phi[n(\rho + 1)] = \begin{cases} \frac{1}{[n(\rho+1)+1]} \left[\frac{n(\rho+1)}{n(\rho+1)+1}\right]^{k-n(\rho+1)}, & k \geq n(\rho + 1). \\ 0, & \text{otherwise.} \end{cases} \quad (26)$$

Note that when  $n = 2$  this result reduces to that in Eq. (10). To check the accuracy of Eq. (26), we estimate the degree distribution of  $ILPHVG_n(\rho)$  associated with  $N \times N$  random matrices whose entries are *i.i.d.* uniform random variables  $U[0, 1]$ . To illustrate the finite size effects, we also define the cutoff value. When  $k > k_0$  all the degree distributions of the numerical results are smaller than the theoretical result in Eq. (26), and  $k_0$  is the cutoff value. Figs. 7(a) and 7(c) show semi-log plots of the finite size degree distributions of  $ILPHVG_4(\rho)$  and  $ILPHVG_8(\rho)$  with  $N = 200$ . Note that the distributions agree with Eq. (26) when  $k \leq k_0$ . To assess the convergence speed of Eq. (26) for finite  $N$ , we estimate the cutoff value  $k_0$  under different finite  $N$  sizes [see Figs. 7(b) and 7(d)]. Note that the location of the cutoff value  $k_0$  scales logarithmically with the system size  $N$ , i.e., finite size effects only affect the tail of the distribution, which quickly converges logarithmically with  $N$ .

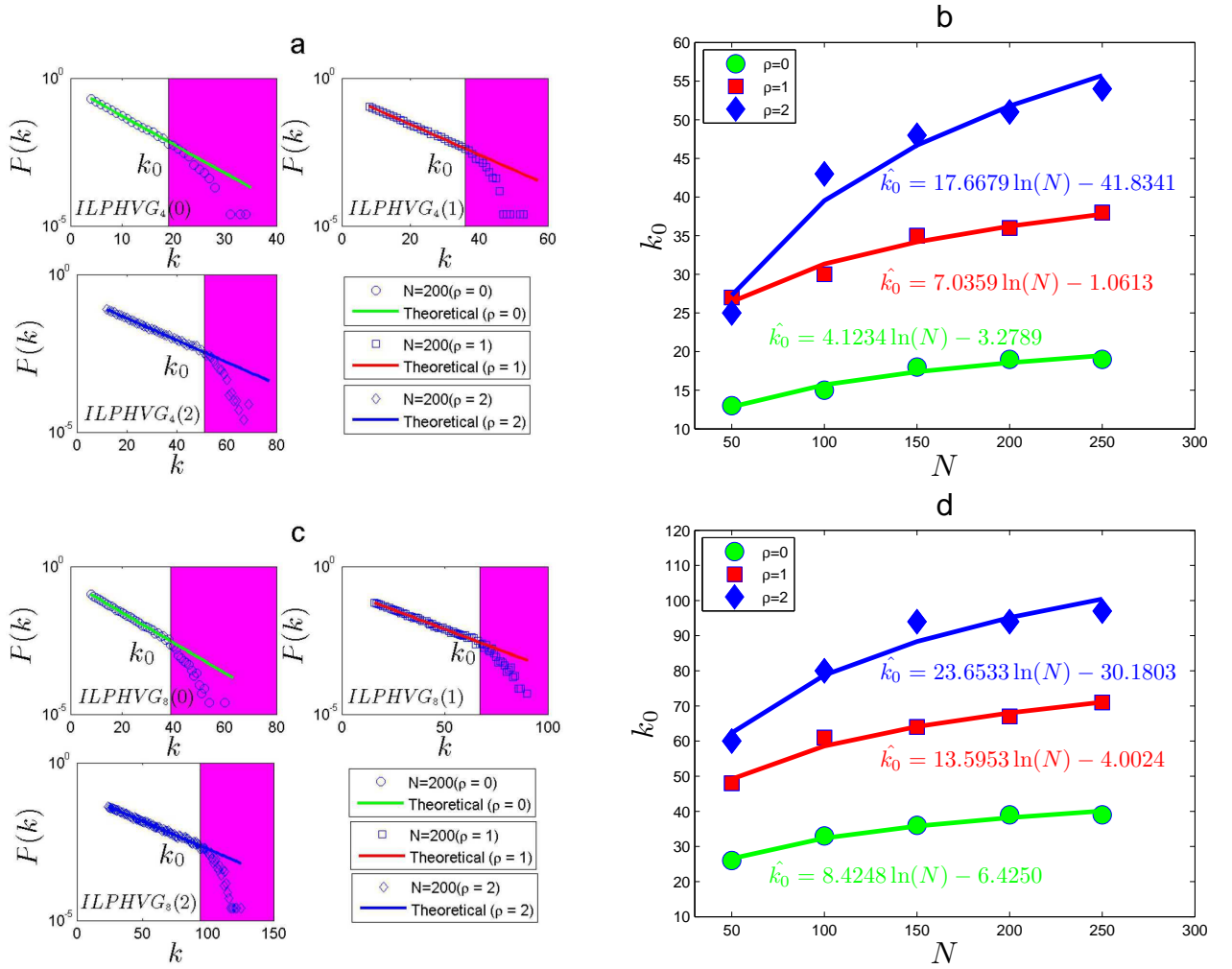


FIG. 7: ( a ) Semi-log plot of the degree distribution of  $\text{ILPHVG}_4(\rho)$  associated to  $N \times N$  random matrices. The solid line is the theoretical value of  $P(k)$  given by Eq. (26). In every case we find excellent agreement with Eq. (26) for  $k \leq k_0$ , where  $k_0$  is a cutoff value that denotes the onset of finite size effects. ( b ) plot of the cutoff  $k_0$  as a function of different size  $N$ , suggesting a logarithmic scaling. ( c ) semi-log plot of the degree distribution of  $\text{ILPHVG}_8(\rho)$  associated to  $N \times N$  random matrices. The solid line is the theoretical value of  $P(k)$  given by Eq. (26). In every case we find excellent agreement with Eq. (26) for  $k \leq k_0$ . ( d ) plot of the cutoff  $k_0$  as a function of different size  $N$ , suggesting a logarithmic scaling.

#### IV. APPLICATION OF $\text{DLPHVG}(\rho)$ AND $\text{ILPHVG}_n(\rho)$

We use the analytical results of  $\text{LPHVG}(\rho)$  to distinguish between random and chaotic signals [34], and we describe the global evolution of crude oil futures. We also describe applications of  $\text{DLPHVG}(\rho)$  and  $\text{ILPHVG}_n(\rho)$ .

**Measure real-valued time series irreversibility by  $\text{DLPHVG}(\rho)$ .** Time series irreversibility is an important topic in basic and applied science [35]. Over the past decade several methods of measuring time irreversibility have been proposed [36–38]. A recent proposal uses the directed horizontal visibility algorithm [39]. Here the Kullback-Leibler divergence (KLD) between the out- and in-degree distributions is defined

$$D[P_{\text{out}}(k)||P_{\text{in}}(k)] = \sum_k P_{\text{out}}(k) \log \frac{P_{\text{out}}(k)}{P_{\text{in}}(k)}. \quad (27)$$

Eq. 27 measures the irreversibility of real-value stationary stochastic series, and we here explore the applicability of  $\text{DLPHVG}(\rho)$ . We first select an appropriate parameter  $\rho$ , map a time series to a directed limited penetrable horizontal visibility graph, and then use Eq. 27 to estimate the degree of irreversibility of the series. Using Theorem 6 and Eq. 27 we find that the KLD between the in- and out-degree distributions associated with an *i.i.d.* random infinite series is equal to zero. Using our analysis of finite size effects, we infer that the KLD between the in- and out-degree distributions associated with an *i.i.d.* random finite series of size  $N$  tends asymptotically to zero. We set  $\rho = 0, 1, \text{ and } 2$ , and calculate the numerical value of the KLD of the random series of 3000 data from uniform, Gaussian, and power-law distributions (see the upper section of Table 1). All numerical values of KLD are approximately 0, which suggests that the *i.i.d.* time series is reversible.

We next examine the chaotic logistic ( $\mu = 4$ ) and Hénon ( $a = 1.4, b = 0.3$ ) map series. Figures 8(a) and 8(b) show plots of the in- and out-degree distributions of  $\text{DLPHVG}(\rho)$ ,  $\rho = 0, 1, 2$  associated with the Logistic map at  $\mu = 4$  and the Hénon map at  $a = 1.4$  and  $b = 0.3$  of 3000 data points. Note that in each case there is a clear distinction between the in- and out-degree distributions, and this differs from the *i.i.d.* series case [see Fig. 6(b)]. We calculate the values of KLD for each case (bottom section of Table 1). We find that the values of KLD are positive and much larger than those of the *i.i.d.* series. Figs. 8(c) and 8(d) show a finite size analysis of the chaotic maps. Note that the KLD values associated with the chaos maps converges with series size  $N$  to a asymptotical nonzero value, which indicates that chaos maps are irreversible.

Thus by selecting an appropriate parameter for  $\rho$ , the  $D[P_{\text{out}}(k)||P_{\text{in}}(k)]$  of  $\text{DLPHVG}(\rho)$  captures the irreversibility of the time series.

TABLE I: Values of the irreversibility measure associated to the degree distribution  $D[P_{\text{out}}(k)||P_{\text{in}}(k)]$  for  $DLPHVG(\rho)$  associated to series of 3000 data generated from reversible and irreversible processes

Series description	$\rho = 0$	$\rho = 1$	$\rho = 2$
Uniform distribution $f(x) = U[0, 1]$	0.000950	0.007106	0.007269
Gaussian distribution	0.002633	0.007106	0.005507
Power law distribution $f(x) \sim x^{-2}$	0.000226	0.004257	0.005267
Logistic map ( $\mu = 4$ )	0.342985	0.090773	0.081985
Hénon map ( $a = 1.4, b = 0.3$ )	0.158358	0.125637	0.140270

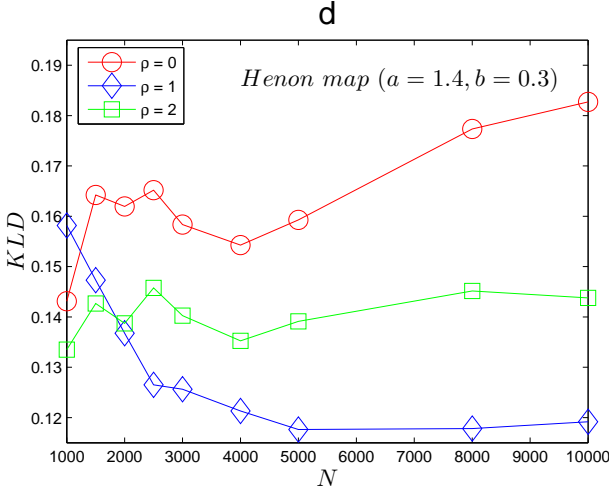
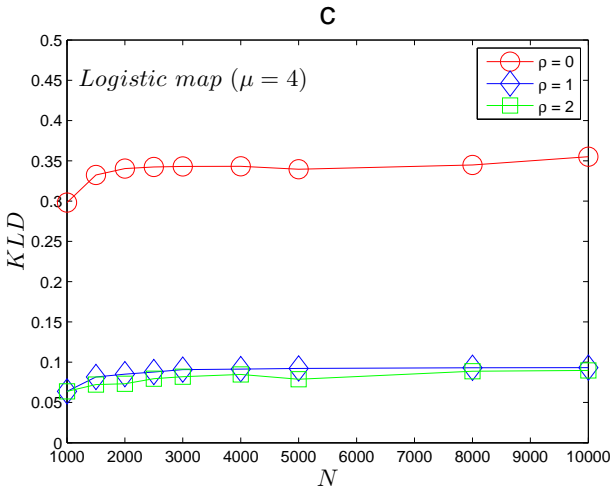
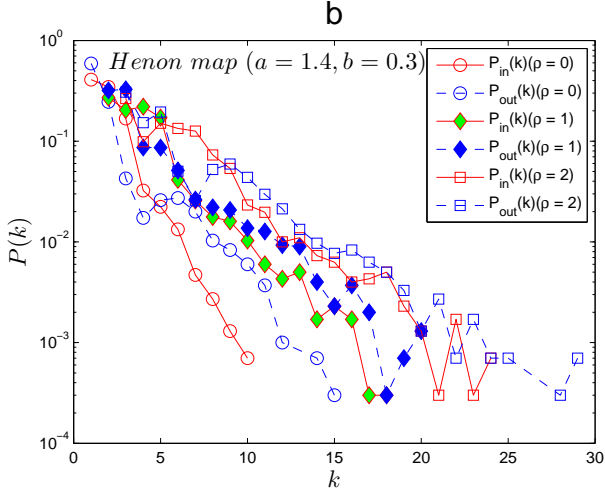
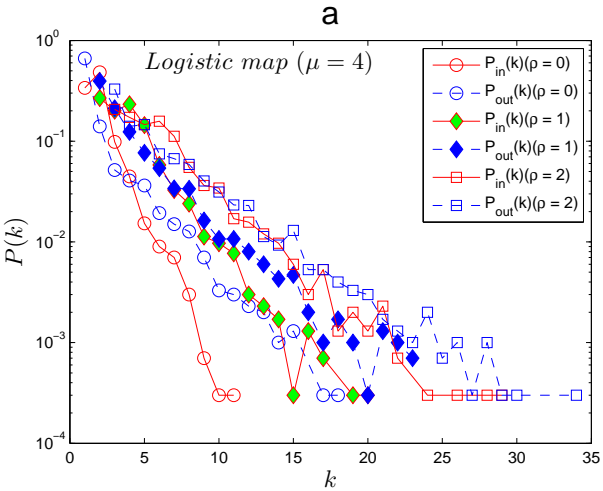


FIG. 8: (a) Plot of the in- and out- degree distributions of DLPHVG( $\rho$ ),  $\rho = 0, 1, 2$  associated to the Logistic map at ( $\mu = 4$ ) of 3000 data points, (b) plot of the in- and out- degree distributions of DLPHVG( $\rho$ ),  $\rho = 0, 1, 2$  associated to the Hénon map at ( $a = 1.4, b = 0.3$ ) of 3000 data points, which different from the uncorrelated cases (see Fig. 6 (b)). (c) the values of  $KLD$  associated to the Logistic map with series size  $N$ , (d) the values of  $KLD$  associated to the Hénon map with series size  $N$ , which converge to a asymptotical nonzero value.

**Discriminating between and chaos using ILPHVG $_n(\rho)$ .** Although chaotic processes display an irregular and unpredictable behavior that is frequently perceived to be random, chaos is a deterministic process that often hides patterns that can be extracted using appropriate techniques. In recent decades research efforts to distinguish between noise and chaos have been widespread [40], and applications have been developed in all scientific disciplines involving complex, irregular empirical signals. Lacasa et al. [33] used visibility graphs to distinguish spatiotemporal chaos from simple randomness. We here also examine spatially extended structures, and we explore whether ILPHVG $_n(\rho)$  can distinguish spatiotemporal chaos from simple randomness.

We define  $\mathbf{X}(t)$  to be a two-dimensional square lattice of  $N^2$  diffusively-coupled chaotic maps that evolve in time [33]. In each vertex of this coupled map lattice (CML) we allocate a fully chaotic logistic map  $x_{t+1} = Q(x_t)$ ,  $Q(x) = 4x(1 - x)$ , and the system is then spatially coupled,

$$\mathbf{X}_{ij}(t+1) = (1 - \epsilon)Q[\mathbf{X}_{ij}(t)] + \frac{\epsilon}{4} \sum_{i',j'} Q[\mathbf{X}_{i'j'}(t)], \quad (28)$$

where the sum extends to the Von Neumann neighborhood of  $ij$  (four adjacent neighbors). The update is parallel, we use periodic boundary conditions, and the coupling strength is  $\epsilon \in [0, 1]$ . Fig. 9(a) shows a semi-log plot for  $N = 200$  of the degree distribution of ILPHVG $_8(\rho)$ ,  $\rho = 0, 1, 2$  associated with a two-dimensional uncorrelated random field of uniform random variables (stars), and a two-dimensional coupled map lattice of diffusively coupled fully chaotic logistic maps for the coupling constants  $\epsilon = 0$  (squares), and  $\epsilon = 0.1$  (diamonds). Figure 9(b) shows a plot of the degree distribution of ILPHVG $_8(\rho)$ ,  $\rho = 0, 1, 2$  associated with the two-dimensional coupled map lattices of diffusively coupled fully chaotic logistic maps with a coupling constant  $\epsilon = 0.7$ . Eq. (26) shows  $\rho = 0$  (green line),  $\rho = 1$  (red line), and  $\rho = 2$  (pink line).

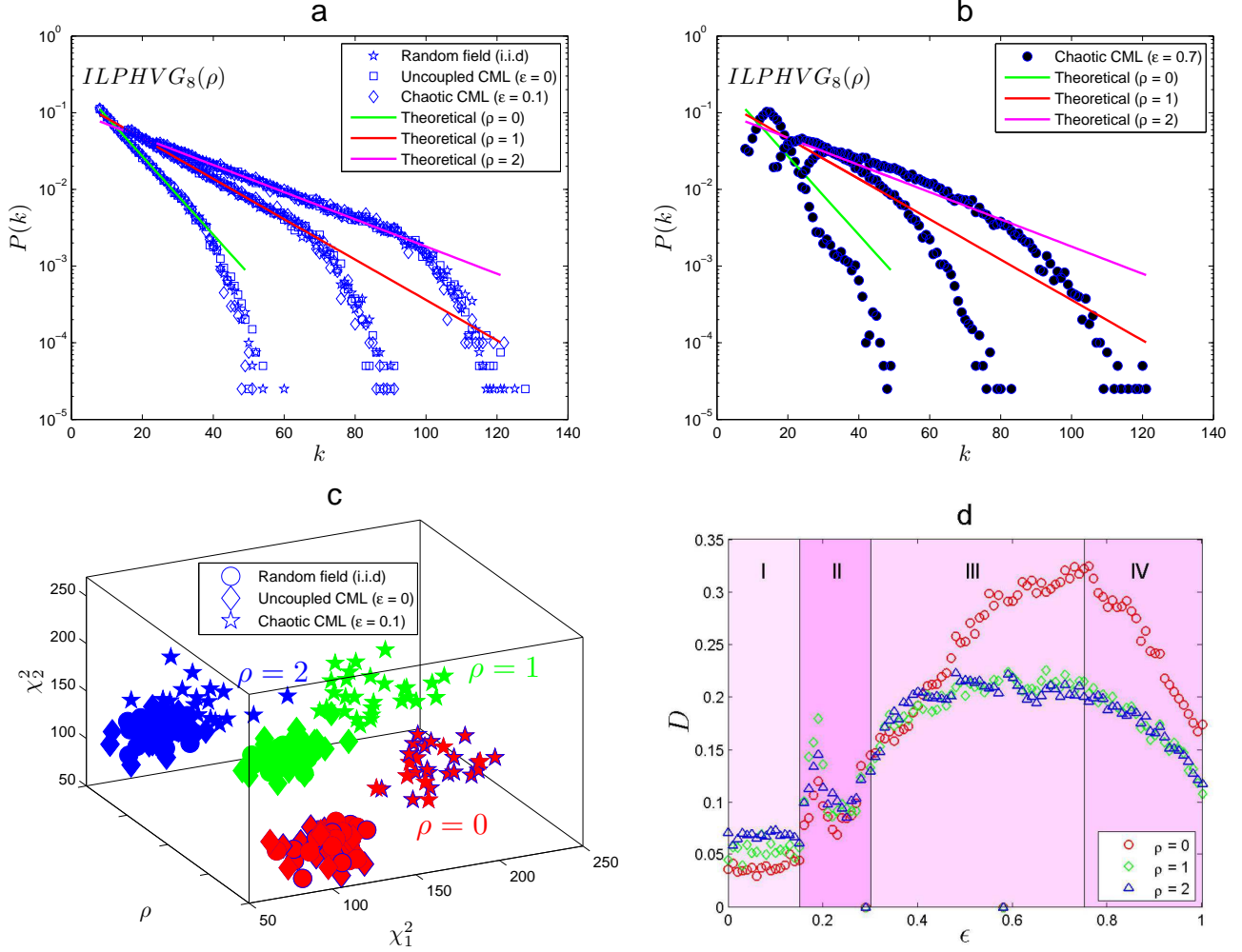


FIG. 9: (a) Semi-log plot of the degree distribution of  $ILPHVG_8(\rho)$ ,  $\rho = 0, 1, 2$  associated to a two-dimensional uncorrelated random field of uniform random variables (stars), and two-dimensional coupled map lattices of diffusively coupled fully chaotic logistic maps, for coupling constant  $\epsilon = 0$  (squares) and  $\epsilon = 0.1$  (diamonds). The solid green line is Eq. (26) for  $\rho = 0$ , the solid red line for  $\rho = 1$ , and the solid pink line for  $\rho = 2$ , (b) semi-log plot of the degree distribution of  $ILPHVG_8(\rho)$ ,  $\rho = 0, 1, 2$  associated to two-dimensional coupled map lattices of diffusively coupled fully chaotic logistic maps, for coupling constant  $\epsilon = 0.7$  (black dots), (c) the  $\chi^2$  statistic in two dimensions phase space (let time delay  $\tau = 2$ ), (d) scalar parameter  $D$  as a function of the coupling constant  $\epsilon$ , computed from the degree distribution of  $ILPHVG_8(\rho)$ ,  $\rho = 0, 1, 2$  associated to  $100 \times 100$  CMLs of fully chaotic logistic maps.

Figs. 9(a) and 9(b) show that the degree distribution of  $ILPHVG_8(\rho)$ ,  $\rho = 0, 1, 2$  associated with the uncoupled ( $\epsilon = 0$ ) and weakly coupled ( $\epsilon = 0.1$ ) cases is indistinguishable from the degree distribution associated with the *i.i.d.* random field. Fig. 9(b) shows that the degree distribution deviates from the theoretical result in Eq. (26) only in the strongly coupled case ( $\epsilon = 0.7$ ). Note that the coupled map lattices from Eq. (28) when  $\epsilon > 0$  spatial correlations settle in and the degree distributions of  $ILPHVG_8(\rho)$  are statistically different from the theoretical result in Eq. (26), but the degree distribution of  $ILPHVG_8(\rho)$ ,  $\rho = 0, 1, 2$  associated with the *i.i.d.* random field, the uncoupled case ( $\epsilon = 0$ ), and the weakly coupled case ( $\epsilon = 0.1$ ) are well approximated by Eq. (26)



in each case. There are deviations for  $k > k_0$  ( $k_0 = 19$  for  $\rho = 0$ ,  $k_0 = 36$  for  $\rho = 1$ , and  $k_0 = 51$  for  $\rho = 2$ ) but they are caused by finite size effects (see Fig. 7). To quantify potential deviations of the uncoupled ( $\epsilon = 0$ ) and weakly coupled ( $\epsilon = 0.1$ ) cases from Eq. (26), we compute  $\chi^2$

$$\chi^2 = N^2 \sum_k \frac{[P_{\text{num}}(k) - P_{\text{theo}}(k)]^2}{P_{\text{theo}}(k)} \quad (29)$$

where  $P_{\text{num}}(k)$  is the degree distribution of the numerical result and  $P_{\text{theo}}(k)$  the theoretical result from Eq. (26). Here we consider 30 realizations of the *i.i.d.* random field, the uncoupled map lattices ( $\epsilon = 0$ ), and the weakly coupled map lattices ( $\epsilon = 0.1$ ), and in each case we use  $8 \leq k \leq 44$  for  $\rho = 0$ ,  $16 \leq k \leq 77$  for  $\rho = 1$ , and  $24 \leq k \leq 99$  for  $\rho = 2$  to compute the  $\chi^2$  statistic that measures the deviation between the empirical degree distribution and the theoretical result. Fig. 9(c) shows the calculated results in a two-dimensional phase space with a time delay  $\tau = 2$ . Note that there are clear distinctions between the uncorrelated *i.i.d.* random field, the uncoupled map lattices ( $\epsilon = 0$ ), and the weakly coupled map lattices ( $\epsilon = 0.1$  for  $\rho = 0$  and  $\rho = 1$ ), but when  $\rho = 2$  the distinction is no longer clear. We thus select an appropriate parameter  $\rho$  and use the degree distribution of ILPHVG( $\rho$ ) to distinguish noise from chaos.

Note that when we increase the coupling constant  $\epsilon$  the spatiotemporal dynamics of the coupled map lattice shows a rich phase diagram. Using the degree distribution of ILPHVG<sub>8</sub>( $\rho$ ), we show this rich spatiotemporal dynamics process. For each  $\epsilon$  we compute the degree distribution of the associated ILPHVG<sub>8</sub>( $\rho$ ). We then compute the distance  $D$  between the degree distribution at  $\epsilon$  and the corresponding result for  $\epsilon = 0$  in Eq. (26),

$$D = \sum_k |P_\rho(k) - \frac{1}{8\rho+9} (\frac{8\rho+8}{8\rho+9})^{k-8(\rho+1)}|, \quad (30)$$

where  $P_\rho(k)$  is the degree distribution of ILPHVG<sub>n</sub>( $\rho$ ), and  $D$  is a scalar order parameter that describes the spatial configuration of the CML. Figure 9(d) shows that when  $\rho = 0, 1, 2$  the evolutions of  $D$  with  $\epsilon$  changes from 0 to 1, indicating sharp changes in the different phases—fully developed turbulence with weak spatial correlations (I), periodic structure (II), spatially coherent structure (III), and mixed structure (IV)—between periodic and spatially-coherent structures [33]. Thus the degree distribution of the ILPHVG<sub>8</sub>( $\rho$ ) can capture the rich spatial structure.

## V. DISCUSSIONS

We have introduced a directed limited penetrable horizontal visibility graph DLPHVG( $\rho$ ) and an image limited penetrable horizontal visibility graph (ILPHVG<sub>n</sub>( $\rho$ )), both inspired by the limited penetrable horizontal visibility graph LPHVG( $\rho$ ) [34]. These two algorithms are expansions of the limited penetrable horizontal visibility algorithm. We first derive theoretical results on the topological properties of LPHVG( $\rho$ ), including degree distribution  $P(k)$ , mean degree  $\langle k \rangle$ , the relation between the datum height  $x$  and the mean degree  $\langle K(x) \rangle$  of the nodes associated to data with a height equal to  $x$ , the normalized mean distance  $\langle d \rangle$ , the local clustering coefficient distribution  $P(C_{\text{min}})$  and  $P_{\text{max}}$ , and the probability of long distance visibility  $P_\rho(n)$ . We then deduce the in- and out-degree distributions  $P_{\text{in}}(k)$  and  $P_{\text{out}}(k)$  of DLPHVG( $\rho$ ), and the degree distribution of ILPHVG<sub>n</sub>( $\rho$ ). We perform several numerical simulations to check the accuracy of our analytical results. We then present applications of the directed limited penetrable horizontal visibility graph and the image limited penetrable horizontal visibility graph, including measuring the irreversibility of a real-value time series and discriminating between noise and chaos, and empirical results testify to the efficiency of our methods.

Our theoretical results on topological properties are an extension of previous findings [22, 32–34]. In the structure of the limited penetrable horizontal visibility graph family, the limited penetrable parameter  $\rho$  is a important and affects the structure

of the associated graphs. Under certain parameter  $\rho$  values, the exact results of the associated graphs reveals the essential characteristics of the system, e.g., when  $\rho = 0$  and  $\rho = 1$ , using the degree distribution of  $ILPHVG_8(\rho)$  we can distinguish between uncorrelated and weakly coupled systems, but when  $\rho = 2$  the distinction is no longer clear [see Fig. 9 (c)]. Open problem for future research include how to use real data in selecting an optimal limited penetrable parameter  $\rho$ , and how to further apply the limited penetrable horizontal visibility graph family.

## VI. ACKNOWLEDGMENTS

The Research was supported by the following foundations: The National Natural Science Foundation of China (71503132, 71690242, 91546118, 11731014, 71403105, 61403171), Qing Lan Project of Jiangsu Province (2017), University Natural Science Foundation of Jiangsu Province (14KJA110001), Jiangsu Center for Collaborative Innovation in Geographical Information Resource Development and Application, CNPq, CAPES, FACEPE and UPE.

- 
- [1] Z. K. Gao, M. Small, J. Kurths, *Europhys. Lett.*, 116(5): 50001 (2017).
  - [2] J. Zhang, M. Small, *Phys. Rev. Lett.*, 96(23): 238701 (2006).
  - [3] L. Lacasa, B. Luque, F. Ballesteros, et al., *Proc. Natl. Acad. Sci.*, 105(13): 4972-4975 (2008).
  - [4] N. Marwan, J. F. Donges, Y. Zou, et al., *Phys. Lett. A*, 373(46): 4246-4254 (2009).
  - [5] A. H. Shirazi, G. R. Jafari, J. Davoudi et al., *J. Stat. Mech. Theor. Exp.*, 2009(07): P07046 (2009).
  - [6] Y. Zhao, T. Weng, S. Ye, *Phys. Rev. E*, 90(1): 012804 (2014).
  - [7] J. F. Donges, Y. Zou, N. Marwan et al., *Europhys. Lett.*, 87(4): 48007 (2009).
  - [8] V. Stolbova, P. Martin, B. Bookhagen et al., *Nonlinear Process Geophys.*, 21(4): 901-917 (2014).
  - [9] Wang M, Tian L. *Physica A*, 461: 456-468 (2016).
  - [10] C. Zhou, L. Ding, M.J. Skibniewski, et al., *Saf. Sci.*, 98: 145-158 (2017).
  - [11] P. Oświecimka, L. Livi, S. Drożdż, *Phys. Rev. E*, 94(4): 042307 (2016).
  - [12] Z.K. Gao, S. Li, W.D. Dang, et al., *Int. J. Bifurc. Chaos*, 27(08): 1750123 (2017).
  - [13] M. Wang, Y. Chen, L. Tian et al., *Applied Energy*, 175: 109-127 (2016).
  - [14] M. Wang, L. Tian, R. Du, *Applied Energy*, 180: 779-791 (2016).
  - [15] M. Wang, L. Tian, H. Xu et al., *Physica A*, 473: 188-204 (2017).
  - [16] H. Chen, L. Tian, M. Wang et al., *Sustainability*, 9(4): 574 (2017).
  - [17] R. Du, Y. Wang, G. Dong et al., *Applied Energy*, 196: 142-151 (2017).
  - [18] R. Du, G. Dong, L. Tian et al., *PloS one*, 11(10): e0162362 (2016).
  - [19] J. Xiao, M. Wang, L. Tian et al., *Physica A*, 490: 664-680 (2018).
  - [20] Y. Li, D. Yang, X. Li, *Journal of Mathematical Finance*, 7(03): 734 (2017).
  - [21] I.V. Bezsudnov, A.A. Snarskii, *Physica A*, 414: 53-60 (2014).
  - [22] B. Luque, L. Lacasa, F. Ballesteros et al., *Phys. Rev. E*, 80(4): 046103 (2009).
  - [23] L. Lacasa, B. Luque, J. Luque et al., *Europhys. Lett.*, 86(3): 30001 (2009).
  - [24] R. Ray, M.H. Khondekar, K. Ghosh et al., *Theor. Appl. Climatol.*, 124(1-2): 119-128 (2016).
  - [25] G. Gutin, T. Mansour, S. Severini, *Physica A*, 390(12): 2421-2428 (2011).
  - [26] T.T. Zhou, N.D. Jin, Z.K. Gao et al., *Acta. Phys. Sin.*, 61(3), 030506 (2012).
  - [27] Z.K. Gao, L.D. Hu, T.T. Zhou et al., *Acta. Phys. Sin.*, 62(11), 110507 (2013).

- [28] Z.K. Gao, Q. Cai, Y.X. Yang et al., *Sci. Re.*, 6: 35622 (2016).
- [29] J. Wang, C. Yang, R. Wang et al., *Physica A*, 460: 174-187 (2016).
- [30] R.X. Wang, J.M. Gao, Z.Y. Gao et al., *Sci. China Technol. Sc.*, 59: 604-617 (2016).
- [31] B. Luque, L. Lacasa, F.J. Ballesteros et al., *Chaos*, 22(1): 013109 (2012).
- [32] L. Lacasa, *Nonlinearity*, 27(9): 2063 (2014).
- [33] L. Lacasa, J. Iacovacci, arXiv preprint arXiv:1702.07813, (2017).
- [34] M. Wang, A. L. M. Vilela, R. Du et al., arXiv preprint arXiv: 1710.09877, (2017).
- [35] R. Kawai, J.M.R. Parrondo, C. Van den Broeck, *Phys. Rev. Lett.*, 98(8): 080602 (2007).
- [36] M. Costa, A. L. Goldberger, C. K. Peng, *Phys. Rev. Lett.*, 95(19): 198102 (2005).
- [37] D. Andrieux, P. Gaspard, S. Ciliberto et al. *Phys. Rev. Lett.*, 98(15): 150601 (2007).
- [38] M.B. Kennel, *Phys. Rev. E*, 69(5): 056208 (2004).
- [39] L. Lacasa, A. Nuñez, Roldán É et al., *Eur. Phys. J. B*, 85(6): 217 (2012).
- [40] O.A. Rosso, H.A. Larrondo, M.T. Martin et al., *Phys. Rev. Lett.*, 99(15): 154102 (2007).